Soft Matter

RSC Publishing

PAPER

View Article Online
View Journal | View Issue

Cite this: *Soft Matter*, 2013, **9**, 10779

Dye exchange in micellar solutions. Quantitative analysis of bulk and single molecule fluorescence titrations†

Lucas Piñeiro, Sonia Freire, Jorge Bordello, Mercedes Novo and Wajih Al-Soufi*

Received 2nd August 2013
Accepted 16th September 2013

DOI: 10.1039/c3sm52092g

www.rsc.org/softmatter

A quantitative empirical model is presented, which relates the total surfactant concentration with the fluorescence intensity and the mean translational diffusion coefficient of dyes in micellar solutions, as determined by Fluorescence Correlation Spectroscopy (FCS). Based on this model a systematic data analysis method is defined for the precise determination of the dye binding equilibrium constant, the critical micelle concentration, the translational diffusion coefficients, and the hydrodynamic radii of dyes and micelles and related properties. The method can be used for the routine and automatic determination of the *cmc* of surfactant solutions. The model is applied to dyes with very different hydrophobicity in aqueous solutions of the non-ionic surfactant Triton X-100. As a reference the *cmc* of Triton X-100 is also determined directly from changes in the absorbance of its phenyl-ring applying a ratiometric method.

Introduction

Surfactants are of utmost importance in innumerable industrial applications, pharmaceutical formulations, biochemical protocols, and physiological functions.[1,2] Surfactant aggregation and the formation of micelles above the critical micelle concentration (*cmc*) is itself a fascinating example of spontaneous self-assembly. Micelles can serve as models for specific aspects of other microheterogeneous structures such as lipid membranes,[3] nano-therapeutic systems[4] or primitive cells.[5] Although long known and well-studied, surfactant chemistry is still a vivid field with a huge number of contributions each year.

The study of the dynamic dye-exchange equilibrium in micellar solutions is important for several reasons. First, dyes are well accessible model compounds for other solubilizates in surfactant solutions. The binding equilibrium constant and the rate constants of the exchange of solubilizates between the aqueous and the micellar pseudo-phases are of great interest.[6–8] Second, dye probe molecules are widely used for the characterization of surfactant solutions.[9–11] Fluorescence intensity titration is a sensitive method for the determination of the dye binding constant K, the *cmc* or the aggregation number n.

Fluorescence correlation spectroscopy (FCS), a single molecule technique, yields the translational diffusion constant of a dye in micellar solution and the relaxation rate constant of the binding of a dye to the micelles.[8,12–18] From this information one can derive the *cmc*, n, K, the hydrodynamic radii of both dye and micelle,[12–16] and also the dye exchange rate constants,[8,17,18] which is a valuable dynamic information not easily accessible with other techniques.

The interaction between dye and surfactant molecules depends on their electrical charge and the hydrophobicity of the dye. Strong interaction due to electrostatic attraction or strong dye hydrophobicity leads to the formation of dye-surfactant aggregates, ionic pairs and distortions in the native surfactant aggregation as probed by the dye.[19–23] A dye with only moderate hydrophobicity and no electrostatic interaction (neutral dye or surfactant) helps to avoid these complications, but implies that the dye will be partitioned between the aqueous and the micellar environments.

The correct analysis and interpretation of the data obtained from dye probes requires a detailed understanding of the fast dye exchange equilibrium in the micellar solution. A dye molecule constantly exchanges between the aqueous and the micellar environments. The fraction of the time a dye molecule is free or bound, or, which is equivalent, the molar fractions of free and bound dye, depends on the binding equilibrium constant and on the micelle concentration. It is generally not correct to assume that at concentrations immediately above the *cmc* all dye molecules are located within micelles or to treat the fractions of free dye and of dye located in micelles as two static species in FCS measurements. Therefore, when dyes are used for the characterization of a surfactant solution, for example for the determination of the *cmc*, it is imperative to take the dye exchange equilibrium into account.

Departamento de Química Física, Facultade de Ciencias, Universidade de Santiago de Compostela, E-27002 Lugo, Spain. E-mail: wajih.al-soufi@usc.es; m.novo@usc.es; Fax: +34 982824001; Tel: +34 982824114

† Electronic supplementary information (ESI) available: Additional figures and fitting functions. See DOI: 10.1039/c3sm52092g

Beside the chemical structure and the electrical charge of a surfactant, the *cmc* is probably the most important property used for its characterization. The *cmc* is rather qualitatively defined as the surfactant concentration at the onset of the formation of micelles, experimentally observed by a significant change in some measured property. The lack of a theoretical model for the concentrations of surfactant monomers and micelles in solution makes it difficult to establish a quantitative definition of the *cmc*-value, valid for different techniques. A very common procedure to determine the *cmc* from experimental data is to look for the intersection of two straight lines traced through plots of the measured property *versus* the surfactant concentration. This visual data analysis method is highly subjective and can lead to very different *cmc* values depending on the type of representation, the quality of the data and the chosen interval around the *cmc*.[24] As an alternative, we recently presented a compact empirical model for the concentrations of monomeric and micellised surfactants in solution, which establishes a well-defined analytical definition of the *cmc*, independent from the technique. We applied it successfully to experimental data from electrical conductivity, surface tension, NMR chemical shift and to self-diffusion coefficient data of different surfactants.[25] It allowed us to estimate the micellar concentration also around the *cmc* which has been so far not easily accessible with other models. In this contribution we will extend this concentration model to the quantitative analysis of the dye exchange equilibrium in micellar solutions, which is otherwise difficult to achieve, especially near the *cmc*.

One objective of this contribution is to discuss the influence of the dye exchange equilibrium on the *cmc* determined from fluorescence titrations and to propose a systematic data analysis method that takes the binding equilibrium of the dye into account. We apply the method to dyes with very different hydrophobicity and analyse the fluorescence emission and the translational diffusion coefficient determined by FCS. The proposed method can be easily used for routine and automatic determination of the *cmc* and related properties.

This paper deals with a typical non-ionic surfactant, Triton X-100 (TX100), which has been widely studied. TX100 is a good example for the inconsistency in the values reported for micellar properties. For example, for the *cmc* at 25 °C, values between 0.16 mM[26] and 0.6 mM[27] can be found, depending on the technique and the type of data analysis used. In forthcoming contributions we will consider the electrostatic interactions between charged dyes and ionic surfactants and the special case of pyrene as a probe.

Theory

In order to describe quantitatively the concentrations of the species involved in a dye-surfactant system three processes have to be analysed: (1) the formation of micelles from surfactant molecules, (2) the partition of the dye molecules between the aqueous solution and the micellar pseudo-phase, and (3) the distribution of the fraction of bound dye molecules among the micelles.

Monomer and micellar concentrations in surfactant solutions

The formation of micelles above the critical surfactant concentration (*cmc*) is a spontaneous and highly dynamic process.[7] There is no established and practical quantitative theory for the concentrations of monomeric and micellised surfactants in solution at a given total surfactant concentration. We therefore use an empirical model for these concentrations near the *cmc*.[25]

Starting point is the "Phillips-condition" which defines the *cmc* as the total surfactant concentration $[S]_0$ at which the change in the gradient of the monomer concentration $[S_1]$ with respect to $[S]_0$ is maximum, that is where the third derivative of $[S_1]$ is zero:[28]

$$\left(\frac{d^3[S_1]}{d[S]_0^3}\right)_{[S]_0=cmc} = 0 \tag{1}$$

Following García-Mateos[29] we then describe the second derivative of $[S_1]$ with respect to $[S]_0$ by a Gaussian function centred at the *cmc*, with amplitude A and width σ:

$$\frac{d^2[S_1]}{d[S]_0^2} = \frac{-A}{\sqrt{2\pi}\sigma} e^{-\frac{([S]_0-cmc)^2}{2\sigma^2}} \tag{2}$$

The standard deviation σ (half width at $e^{-1/2}$) is a measure of the width of the micellar transition region around the *cmc*. In this interval, the concentration of surfactant monomers is still not saturated, but already first micelles are formed (see Fig. 2 below). The smaller the σ the sharper is the transition between the two linear regions below and above the *cmc*.

In order to facilitate the comparison of micellar transition widths σ of surfactants with different *cmc* values, we define the relative micellar transition width r:

$$r = \sigma/cmc \tag{3}$$

After double integration of eqn (2) we obtain eqn (4) as an empirical model for the monomer concentration $[S_1]$ as a function of the total surfactant concentration $[S]_0$.[25]

$$[S_1] = cmc\left[1 - \frac{A}{2}\left(\sqrt{\frac{2}{\pi}} r e^{-\frac{(s_0-1)^2}{2r^2}} + (s_0-1)\left(\mathrm{erf}\left(\frac{s_0-1}{\sqrt{2}r}\right) - 1\right)\right)\right] \tag{4}$$

with the abbreviation $S_0 = [S]_0/cmc$ and the amplitude A:

$$A = \frac{2}{1 + \sqrt{\frac{2}{\pi}} r e^{-\frac{1}{2r^2}} + \mathrm{erf}\left(\frac{1}{\sqrt{2}r}\right)} \tag{5}$$

The concentration of aggregated (micellised) surfactants, $[S_m]$, is the difference between the total surfactant concentration and that of monomeric surfactants:

$$[S_m] = [S]_0 - [S_1] \tag{6}$$

The concentration of micelles, [M], depends on the mean aggregation number, n:

$$[\mathrm{M}] = [\mathrm{S_m}]/n \tag{7}$$

The model assumes a constant aggregation number n, also at the onset of micelle formation around the *cmc*. This is in line with simulations[30] and thermodynamic models[31] and proved to describe well the behaviour of several surfactants.[25]

Eqn (4)–(7) form an excellent concentration model for the description of the properties of a surfactant solution around the *cmc*.[25] This model can be easily plugged into equations that describe derived properties obtained with different techniques, such as eqn (9), (26), (16), and (23). The resulting models can be easily implemented as fit-functions in commercial analysis software. Functions for OriginPro (OriginLab Corporation, USA) are given in the ESI† and can be downloaded from the webpage of the authors.

Binding equilibrium

The exchange of dye molecules between bulk water and micelles is a very fast dynamic process which can be usually well described as a 1 : 1 binding equilibrium applying the mass action model as given in eqn (8), with an apparent (macroscopic) binding equilibrium constant K.[6,7,23]

$$\mathrm{D_f} + \mathrm{M} \overset{K}{\rightleftharpoons} \mathrm{D_b} \quad K = \frac{[\mathrm{D_b}]}{[\mathrm{D_f}][\mathrm{M}]} \tag{8}$$

The molar fractions of free ($\mathrm{D_f}$) and bound dye ($\mathrm{D_b}$) at the total dye concentration $[\mathrm{D}]_0 = [\mathrm{D_f}] + [\mathrm{D_b}]$ are then:

$$X_\mathrm{f} = \frac{[\mathrm{D_f}]}{[\mathrm{D}]_0} = \frac{1}{1 + K[\mathrm{M}]},\ X_\mathrm{b} = \frac{[\mathrm{D_b}]}{[\mathrm{D}]_0} = \frac{K[\mathrm{M}]}{1 + K[\mathrm{M}]} \tag{9}$$

The mean number of dye molecules per micelle (mean occupancy) $\bar{i}$ depends on the concentrations of bound dye and micelles:

$$\bar{i} = \frac{\sum_{i=0}^{\infty} i[\mathrm{M}_i]}{\sum_{i=0}^{\infty} [\mathrm{M}_i]} = \frac{[\mathrm{D_b}]}{[\mathrm{M}]} = [\mathrm{D}]_0 K X_\mathrm{f} \equiv \bar{i}_0 X_\mathrm{f} \tag{10}$$

The mean occupancy $\bar{i}$ decays with increasing surfactant concentration proportional to the fraction of free dye X_f. At very low surfactant concentrations the initial mean occupancy is given by $\bar{i}_0 = [\mathrm{D}]_0 K$, which is constant (see eqn (10)), as both the concentration of bound dye $[\mathrm{D_b}]$ and the micelle concentration [M] tend to zero. The mean occupancy $\bar{i}$ is always smaller than this initial value $\bar{i} \le \bar{i}_0$. Depending on $[\mathrm{D}]_0$ and K, the mean occupancy of the micelles can be high near the *cmc*.

In the equilibrium expression of eqn (8) it is implicitly assumed that the micelle concentration [M] corresponds always to the total micelle concentration. The micelles are not "consumed" in the equilibrium because each micelle can be occupied by more than one dye molecule. We will briefly analyse how this higher occupation affects the experimentally observed equilibrium constant K.

Following Kalyanasundaram[32] we analyse the dye exchange equilibrium between the free dye $\mathrm{D_f}$ and the dye bound to a micelle M_i with a mean occupancy i, described by the equilibrium constant $K_\mathrm{i} = k_+/k_-^{(i)}$ with the association (entry) rate constant k_+ of dye into the micelle and the dissociation (exit) rate constant $k_-^{(i)}$ of any of the i dye molecules in M_i:

$$\mathrm{D_f} + \mathrm{M}_{i-1} \underset{k_-^{(i)}}{\overset{k_+}{\rightleftharpoons}} \mathrm{M}_i \tag{11}$$

Now we assume that both the association rate constant k_+ as well as the dissociation rate constant k_- of each of the i dye molecules in M_i are independent from the occupation number i. This is reasonable because the association process is typically diffusion controlled[7,8,17,18] and the dissociation depends mainly on specific interactions between the dye and the micelle and not on the presence of other dye molecules. Then the dissociation rate constant $k_-^{(i)}$ of any one of the i dye molecules in a micelle M_i is i times that of a dye in a single occupied micelle: $k_-^{(i)} = ik_-$:

$$K_i = \frac{[\mathrm{M}_i]}{[\mathrm{M}_{i-1}][\mathrm{D_f}]} = \frac{k_+}{k_-^{(i)}} = \frac{k_+}{ik_-} \tag{12}$$

With eqn (12) we obtain for the concentration of dye bound to micelles $[\mathrm{D_b}]$:

$$[\mathrm{D_b}] = \sum_{i=1}^{\infty} i[\mathrm{M}_i] = \frac{k_+}{k_-}[\mathrm{D_f}] \underbrace{\sum_{i=1}^{\infty} [\mathrm{M}_{i-1}]}_{=\sum_{i=0}^{\infty}[\mathrm{M}_i]} = \frac{k_+}{k_-}[\mathrm{D_f}][\mathrm{M}] \tag{13}$$

Comparing with eqn (8) we see finally that the observed apparent equilibrium constant $K = k_+/k_-$ is that of the 1 : 1 equilibrium of the addition of a dye molecule to an unoccupied micelle, and that K is independent of the actual occupation number:

$$\frac{k_+}{k_-} = \frac{[\mathrm{D_b}]}{[\mathrm{D_f}][\mathrm{M}]} = K \tag{14}$$

The fact that micelles can be occupied i times is just compensated by the lower effective equilibrium constant $K_i = K/i$ in eqn (11). Therefore eqn (8) and (9) are also valid at high occupation numbers near the *cmc*, as long as the interaction between dye molecules inside the micelle can be neglected. In this case K is independent of [S], [D] and i.

The distribution of bound dye molecules among the micelles is well described by a Poisson distribution.[32,33] The concentrations of micelles which are empty, $[\mathrm{M}_0]$, occupied once $[\mathrm{M}_1]$, or more than once, $[\mathrm{M}_{>1}]$, are given by the respective probabilities:

$$\begin{gathered} P(i) = \frac{[\mathrm{M}_i]}{[\mathrm{M}]} = \frac{\bar{i}^i \mathrm{e}^{-\bar{i}}}{i!} \\ [\mathrm{M}_0] = [\mathrm{M}]P(0) = [\mathrm{M}]\mathrm{e}^{-\bar{i}},\ \ [\mathrm{M}_1] = [\mathrm{M}]P(1) = [\mathrm{M}]\bar{i}\mathrm{e}^{-\bar{i}} \\ [\mathrm{M}_{>1}] = [\mathrm{M}] - [\mathrm{M}_0] - [\mathrm{M}_1] = [\mathrm{M}](1 - (1 + \bar{i})\mathrm{e}^{-\bar{i}}) \end{gathered} \tag{15}$$

Spectral properties

Dye fluorescence spectra. The fluorescence emission intensity of the dye in the binding equilibrium of eqn (8) and (9) is

the sum of the emissions of free and bound dye as given in eqn (16), where $F_f(\lambda)$ and $F_b(\lambda)$ are the respective limiting fluorescence intensities.

$$F(\lambda,\ [S]_0) = F_f(\lambda)X_f + F_b(\lambda)X_b = \frac{F_f(\lambda)}{1+K[M]} + \frac{F_b(\lambda)K[M]}{1+K[M]} \quad (16)$$

FCS. FCS analyses spontaneous fluorescence intensity fluctuations that may be caused by various processes at the molecular level.[17,34,35]

The correlation function for intensity fluctuations due to the translational diffusion G_D of a fluorescent species across the sample volume of a confocal microscope with radial and axial $1/e^2$ radii w_{xy} and w_z, respectively, is given by:

$$G_D(\tau) = \frac{1}{N}\left(1+\frac{\tau}{\tau_D}\right)^{-1}\left(1+\left(\frac{w_{xy}}{w_z}\right)^2\frac{\tau}{\tau_D}\right)^{-\frac{1}{2}} \quad (17)$$

N is the mean number of fluorescent molecules within the sample volume and τ_D is the translational diffusion time (residence time) of the molecules across the sample volume. From τ_D and the radius w_{xy} the translational diffusion coefficient D can be calculated as:

$$D = \frac{{w_{xy}}^2}{4\tau_D} \quad (18)$$

The population of the dark triplet state of the dye leads to an additional exponential term in the correlation curve with an amplitude A_T and a time constant τ_T given by the triplet lifetime of the fluorophore:

$$G_T(\tau) = 1 + A_T\, e^{-\tau/\tau_T} \quad (19)$$

The correlation function of a dye in a micellar solution has been described previously.[8,17,18,36] Under conditions where the micelle concentration [M] is much higher than that of the dye, the dye exchange (eqn (11)) is pseudo-first-order with the relaxation time τ_R of the binding process given by:

$$\tau_R = (k_+[M] + k_-)^{-1} \quad (20)$$

Under the assumption that the relaxation time τ_R of the binding equilibrium is much shorter than the typical diffusion times of free, τ_{Df}, and bound dye, τ_{Db}, (fast dye exchange, $\tau_R \ll \tau_{Df}, \tau_{Db}$), the following correlation function for diffusion, triplet dynamics and binding dynamics is obtained:

$$G(\tau) = \frac{1}{N}\left(1+\frac{\tau}{\bar{\tau}_D}\right)^{-1}\left(1+\left(\frac{w_{xy}}{w_z}\right)^2\frac{\tau}{\bar{\tau}_D}\right)^{-\frac{1}{2}} G_T\left(1+A_R e^{-\tau/\tau_R}\right) \quad (21)$$

where the diffusion term is now defined by a mean diffusion time $\bar{\tau}_D$ and an amplitude that depends on the mean number N of dye molecules in the sample volume (independent of their state or brightness). The relaxation term has relative amplitude A_R and correlation time τ_R.

It is important to realize that the two binding states of the dye (free and bound) will not be resolved by FCS as two distinct species, but as a single one with the mean diffusion coefficient $\bar{D}$, given by the individual diffusion coefficients D_f and D_b, and the molar fractions of free and bound dye (eqn (9)). $\bar{D}$ in turn can be expressed as a function of [M], K, and the limiting diffusion times of free and bound dye τ_{Df} and τ_{Db}, using eqn (9) and (18):

$$\overline{D} = X_f D_f + X_b D_b = \frac{1}{1+K[M]}\frac{{w_{xy}}^2}{4\tau_{Df}} + \frac{K[M]}{1+K[M]}\frac{{w_{xy}}^2}{4\tau_{Db}} \quad (22)$$

This finally leads to the mean diffusion time $\bar{\tau}_D$ in eqn (21):

$$\bar{\tau}_D = \frac{{w_{xy}}^2}{4\overline{D}} = \frac{\tau_{Df}\tau_{Db}(1+K[M])}{\tau_{Db}+\tau_{Df}K[M]} = \frac{\tau_{Df}(1+K[M])}{1+\frac{\tau_{Df}}{\tau_{Db}}K[M]} \quad (23)$$

It is known that the association rate constant k_+ of moderately hydrophobic dyes to micelles is diffusion controlled $k_+ \approx k_d \approx 10^9\ M^{-1}\ s^{-1}$.[7,18] Using eqn (20), this allows one to give an estimate for the upper (slower) limit of the relaxation time τ_R for a dye of the binding equilibrium constant K:

$$\tau_R \leq \tau_R([M]\to 0) = \frac{1}{k_-} = \frac{K}{k_+} \approx \frac{K}{k_d} \approx \frac{K}{10^9\ M^{-1}\ s^{-1}} \quad (24)$$

Ratiometric analysis of surfactant absorbance spectra

Some surfactants show changes in their spectral properties with micellisation. The typically small changes in absorbance are best detected ratiometrically. The absorbance (A) of a surfactant in solution (without dye) at a given wavelength (λ) and total surfactant concentration ($[S]_0$) is the sum of the absorbances of monomeric and micellised surfactant molecules, given by the respective molar absorption coefficients $\varepsilon_1(\lambda)$ and $\varepsilon_m(\lambda)$, the concentrations $[S_1]$ and $[S_m]$, and the absorption path length ℓ:

$$A(\lambda, [S]_0) = [S_1]\varepsilon_1(\lambda)\ell + [S_m]\varepsilon_m(\lambda)\ell \quad (25)$$

The absorbance ratio at two wavelengths λ_a and λ_b is then:

$$q_A([S]_0) = \frac{A(\lambda_b)}{A(\lambda_a)} = \frac{[S_1]\varepsilon_1(\lambda_b)+[S_m]\varepsilon_m(\lambda_b)}{[S_1]\varepsilon_1(\lambda_a)+[S_m]\varepsilon_m(\lambda_a)} = \frac{[S_1]q_1+[S_m]q_m q_a}{[S_1]+[S_m]q_a} \quad (26)$$

with absorbance ratios q_1 and q_m of each species at the two wavelengths, and ratio q_a of the two species at wavelength λ_a:

$$q_1 = \frac{\varepsilon_1(\lambda_b)}{\varepsilon_1(\lambda_a)},\ q_m = \frac{\varepsilon_m(\lambda_b)}{\varepsilon_m(\lambda_a)},\ q_a = \frac{\varepsilon_m(\lambda_a)}{\varepsilon_1(\lambda_a)} \quad (27)$$

The ratio $q_1 = q_A([S]_0 \to 0)$ can be estimated from the absorbance well below the *cmc*. The ratio $q_m = q_A([S]_0 \to \infty)$ is the limit at high concentration. Concentrations $[S_1]$ and $[S_m]$ can be determined from eqn (4)–(7).

Results and discussion

Direct TX100 UV-absorbance

In order to validate the model we use for the concentrations of a monomeric and micellised surfactant (eqn (4)–(7)) we study first a property of the surfactant TX100 itself, without dye and without the need to consider the dye exchange equilibrium. We tested the model before successfully with several ionic surfactants analysing their electrical conductivity,[25] but the neutral TX100 requires a

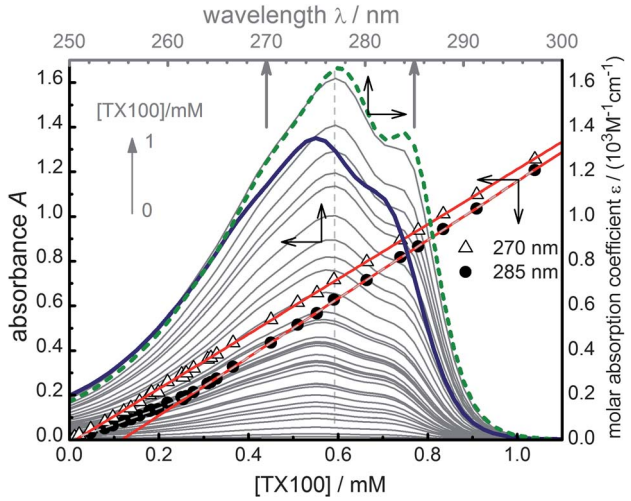

Fig. 1 Absorbance of aqueous solutions of TX100. Thin grey curves: absorbance spectra with [TX100] = 0–1 mM. Thick curves: pure spectra of the molar absorption coefficients ε of monomeric (continuous blue curve) and micellised (dashed green curve) TX100 as obtained from PCGA analysis of the absorbance spectra.[41,42] Symbols: absorbance *vs.* [TX100] at 270 nm (open triangles) and 285 nm (closed circles) and linear fits above 0.3 mM (red straight lines). Small deviations in the baseline of the absorbance spectra due to scattered light at higher TX100 concentrations were corrected.

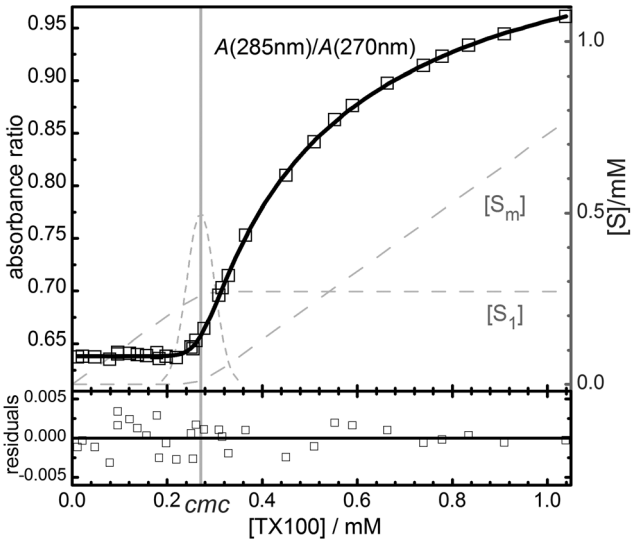

Fig. 2 Absorbance ratio (squares, left scale) $A(285\text{ nm})/A(270\text{ nm})$ of TX100 (data of Fig. 1) and nonlinear fit (thick line) of eqn (26), (4) and (6) with $cmc = 0.270 \pm 0.002$ mM,‡ $r = 0.108 \pm 0.008$, $q_1 = 0.6385$, $q_m = 1.076$ and $q_a = 0.99$. The dashed lines (right scale) are the calculated concentrations of surfactant monomers ($[S_1]$) and of surfactants in micelles ($[S_m]$) (eqn (4)–(6)), and the relative second derivative of $[S_1]$ (eqn (2)) in arbitrary units with a transition width $\sigma = r \times cmc$. The vertical line at $[S]_0 = 0.27$ mM indicates the *cmc*.

different approach. Both the UV-absorbance and the fluorescence of the phenyl ring of TX100 show significant changes around the *cmc*.[37] However, the fluorescence of TX100 is strongly distorted by reabsorption at concentrations at and above the *cmc*, so that its analysis is questionable.[38–40] We use instead the UV-absorbance of TX100, which shows a small but significant bathochromic (red) shift above the *cmc* accompanied by the appearance of a pronounced shoulder at the red edge around 285 nm (grey spectra in Fig. 1). The Lambert–Beer plot of the absorbance at 285 nm *versus* concentration (black symbols in Fig. 1) shows a significant change in its slope around the *cmc*, which is not observed at 270 nm. This change is much better appreciated in the plot of the absorbance ratio at these wavelengths, which shows a strong increase above the *cmc* (Fig. 2). This ratiometric analysis is much less affected by the uncertainties in the TX100 concentration and in the experimental absorbance than the absorbance itself or especially the molar absorbance.

The fit of the absorbance ratio with eqn (26) and (4)–(7) is excellent (Fig. 2), validating the concentration model, especially also around the *cmc*. The value of the ratio q_1 coincides with the one obtained from a linear fit of the absorbances below the *cmc*. The value of the *cmc* = 0.270 ± 0.002 mM matches well the literature value of 0.26 mM.‡[32] The relative transition width r of about 10% is similar to that obtained from conductivity measurements for SDS.[25] The similarity of the relative transition width between SDS and TX100 is striking, given the big differences in their *cmc*, aggregation number and charge (SDS: *cmc* = 8.1 mM, $n = 62$).[25]

‡ The errors indicate only the precision of one standard deviation as obtained from the nonlinear fits. The accuracy of the values is mostly limited by that of the concentration of different TX100 stock solutions (see Experimental section).

The concentration model of eqn (26) and (4)–(7) makes it also possible to apply more detailed data analysis methods, such as principal component analysis (PCA) and global analysis (GA) of the full absorbance (or emission) spectra,[41,42] which give the pure spectra of the molar absorption coefficients ε of monomeric and micellised of TX100 (thick lines in Fig. 1).

Fluorescence titrations

We analyse first the properties of moderately hydrophobic dyes, such as ANS and the coumarins C153 and C152 separately. Then we compare the data of several dyes of very different hydrophobicity and discuss the problems in the use of graphical methods for the determination of the *cmc* and present how to improve the analysis.

ANS in TX100 micelles

The dye 2-anilinonaphthalene-6-sulfonic acid (ANS) and its analogues are well known protein-labelling probes[43] which are nearly nonfluorescent in water but highly fluorescent in nonpolar environments. The high sensitivity of this type of dyes to the solvent polarity and their moderate hydrophobicity make them a good choice for the determination of the *cmc* of micellar solutions.[44–52]

Fig. 3 shows the emission spectra obtained from titrations of ANS with TX100 (thin grey curves). In pure water and below the *cmc* ANS shows only a very weak emission around 425 nm. Above the *cmc* the emission increases strongly and stabilizes only at high TX100 concentrations (see intensity–concentration profiles in Fig. 3). The plot of the fluorescence emission

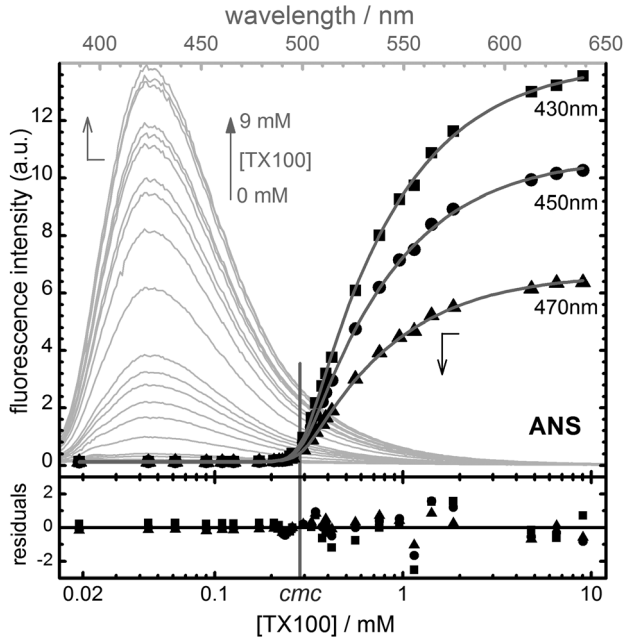

Fig. 3 Fluorescence of ANS in aqueous TX100 solutions with [TX100] = 0–9 mM. Thin grey curves and upper wavelength scale: fluorescence emission spectra. Black symbols and lower concentration scale: fluorescence intensities *vs.* [TX100]. Thick grey curves: global fit of eqn (16) and (4)–(7) at three wavelengths with *cmc* = 0.288 ± 0.005 mM, $r = 0.15 \pm 0.01$, $K = (380 \pm 20)\ 10^3\ M^{-1}$. ($\lambda_{exc} = 350$ nm, $[ANS]_0 = 2 \times 10^{-6}$ M).

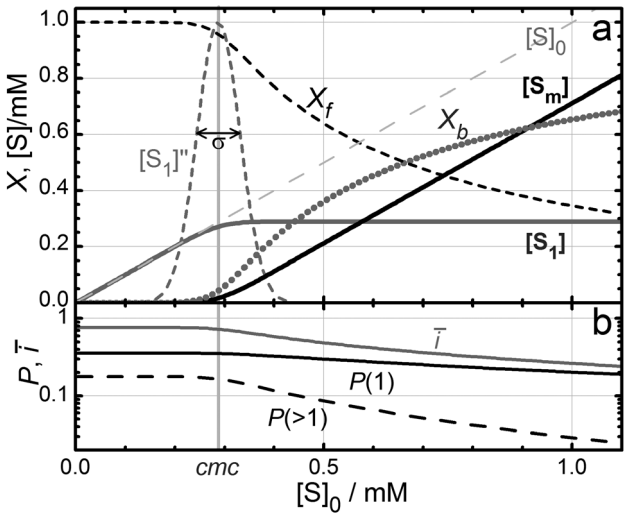

Fig. 4 Calculated properties of ANS/TX100 solutions *versus* the total surfactant concentration ($[S_0]$), with $K = 3.8\ 10^5\ M^{-1}$, $[ANS]_0 = 2 \times 10^{-6}$ M, and $n = 143$. Panel a: fractions of free (X_f) and bound (X_b) dye (eqn (9)) concentrations of surfactant monomers ($[S_1]$) and of surfactants in micelles ($[S_m]$) (eqn (4)–(6)), and relative second derivative of $[S_1]$ (eqn (2)) in arbitrary units. The double arrow corresponds to the transition width $\sigma = r \times cmc$ (eqn (3)). The vertical line at $[S_0] = 0.288$ mM indicates the *cmc*. The thin dashed line represents $[S_0]$ itself. Panel b: occupancy probabilities for one dye per micelle ($P(1)$,black solid line) and for more than one ($P(>1)$, black dashed line), as given by eqn (15), and mean occupancy number $\bar{i}$ (grey solid line).

intensity at one wavelength *versus* the TX100 concentration is curved above the *cmc*, with no clearly linear region, neither in linear nor in logarithmic concentration scales.

The global fit of the concentration model of eqn (4)–(7) together with eqn (16) (fit-functions given in the ESI†) to the intensity–concentration profiles at three wavelengths is excellent (see Fig. 3). The nonlinear fit-parameters K, *cmc*, and r are common to all wavelengths, whereas the linear parameters $F_f(\lambda)$ and $F_b(\lambda)$ are fitted individually. The results are given in Fig. 3. The value *cmc* = 0.288 mM coincides with that determined above from the absorbance of TX100, taking into account the accuracy of about 1% in the concentration of the different stock solutions of TX100.‡ The relative transition width $r = 0.15 \pm 0.01$ is higher than that of the absorbance ratio, but still within the 3σ interval of their precision.

It is instructive to analyse briefly the concentration dependence of some of the properties of the surfactant solution in this titration, as shown in Fig. 4. The high aggregation number, $n = 143$, of TX100 leads to low micellar concentrations as compared to that of the total surfactant. Therefore, the fraction of bound ANS X_b (grey dotted line in Fig. 4, panel a) increases only slowly with increasing surfactant concentration $[S]_0$, in spite of the relatively high binding constant $K = 3.8 \times 10^5\ M^{-1}$. Up to the turning point with $X_f = X_b = 0.5$ at about $[S]_0^{(50\%)} = 0.66$ mM ($[M]^{(50\%)} = K^{-1}$ or $[S]_0^{(50\%)} \approx cmc + n/K$) the fraction of free dye is still higher than that of the bound one. The mean occupancy of micelles with ANS molecules, $\bar{i} = 0.8X_f$ (grey curve in Fig. 4, panel b), is always lower than one, also near the *cmc*.

C152 and C153 in TX100 micelles

The neutral laser dyes coumarin 152 (C152) and coumarin 153 (C153) are typical fluorescent probes sensitive to the polarity and viscosity of their local environment.[53,54] These 7-aminocoumarins have relatively low fluorescence quantum yields in aqueous solution and poor photostability.[55] However, being neutral dyes with relatively high Stokes shifts and a strong increase in fluorescence emission in nonpolar or restrictive microenvironments, C152 and C153 are very interesting probes for the study of heterogeneous systems such as micelles.[18,53]

Fig. 5 shows the fluorescence emission spectra obtained from titrations of C153 with TX100 (grey curves). The corresponding data for C152 can be found in the ESI.† In pure water and below the *cmc* both C153 and C152 show only a very weak emission around 540 nm. Above the *cmc* the emission increases strongly with a significant blue-shift (see intensity–concentration profiles in Fig. 5 and the ESI†). The increase is more pronounced for C153 than for C152.

Eqn (16) and (4)–(7) fit the concentration profiles very well (Fig. 5 and ESI†), also around the *cmc*. The C153 data fit with *cmc* = 0.290 ± 0.005 mM, $r = 0.121 \pm 0.005$ and $K = (970 \pm 20)\ 10^3\ M^{-1}$, and that of C152 with *cmc* = 0.22 ± 0.05 mM, $r = 0.18 \pm 0.13$ and $K = (170 \pm 10)\ 10^3\ M^{-1}$. The *cmc* of C153 coincides well with the values determined before. The low binding equilibrium constant K of C152 makes this dye much less sensitive to the formation of micelles than ANS or C153 and leads to high uncertainties in the determination of the *cmc* and r.

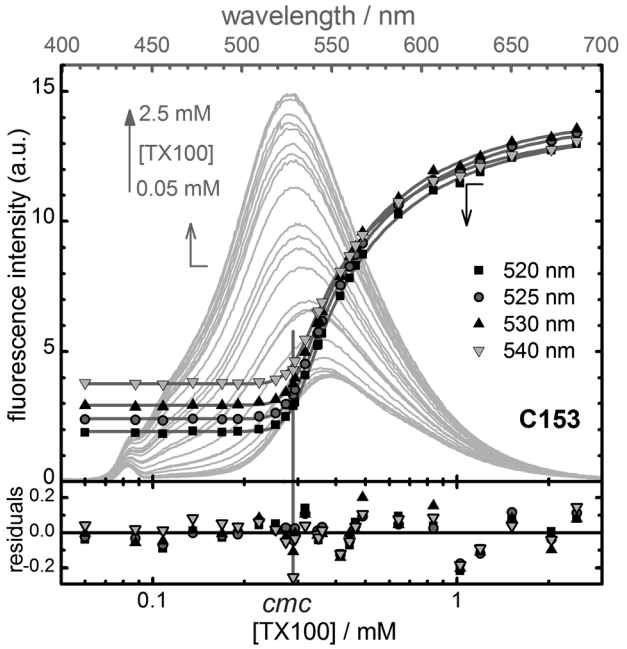

Fig. 5 Fluorescence of C153 in aqueous TX100 solutions with [TX100] = 0.05–2.5 mM. Thin grey curves and upper wavelength scale: fluorescence emission spectra. Black symbols and lower concentration scale: fluorescence intensities *vs.* [TX100]. Thick curves: global fit of eqn (16) and (4)–(7) at four wavelengths with $cmc = 0.290 \pm 0.005$ mM, $r = 0.121 \pm 0.005$, and $K = (970 \pm 20) \times 10^3$ M^{-1}. ($\lambda_{exc} = 380$ nm, $[C153]_0 < 5 \times 10^{-8}$ M, Raman peak around 440 nm).

Comparison of several dyes in exchange with TX100

Fig. 6 shows the normalized fluorescence emission intensity of dyes of different hydrophobicity as a function of TX100 concentration in a logarithmic concentration scale (see the linear concentration scale in the ESI†). The highly hydrophobic dyes Perylene, Pyrene and C153 changed their emission intensity already below the *cmc* of TX100 and reached saturation within the studied concentration range. The less hydrophobic dyes ANS, C152, coumarin 460 (C460) and rhodamine 123 (R123) show practically no change below the *cmc* and reach saturation only at high TX100 concentration. Dyes of very low hydrophobicity such as Pyronine Y need very high TX100 concentrations to show a significant change in emission intensity. All curves can be fitted globally with eqn (16) and the surfactant concentration model (4)–(7) with fixed common values of $cmc = 0.27$ and $r = 0.15$. The results for the binding constants coincide well with those from fits of the individual titration series. The binding constants of the dyes span over several orders of magnitude, from $K = 4 \times 10^3$ M^{-1} in the case of the weakly binding Pyronine Y up to $K = 1 \times 10^7$ M^{-1} of the strongly hydrophobic Perylene (see Table 1). The behaviour of these dyes with very different hydrophobicity can be described with the same model for the binding equilibrium and the surfactant concentrations, with a common *cmc* of the surfactant and without the need to assume that pre-micellar aggregates are formed before the *cmc*, as proposed by other authors.[56–58]

The very high affinities of dyes such as perylene or pyrene to TX100 micelles produce high initial mean occupation numbers $\bar{i}_0 = [D]_0 K$ (eqn (10)) of the micelles near the *cmc* (see Table 1). Interactions between dye molecules bound to the same micelle can cause self-quenching of the dye or the formation of dimers or excimers and can distort the observed fluorescence titration curve. In order to reduce these effects we kept the mean occupation number below one using low dye concentrations in the experiments. However even at the lowest pyrene concentration, we observed quenching of the pyrene fluorescence near the *cmc* due to excimer formation.[32,43] We did not take this effect into account here but indicate for pyrene an apparent binding constant K in Table 1. A more detailed analysis of the rather complex behaviour of the pyrene fluorescence in surfactant solutions will be subject of a forthcoming contribution.

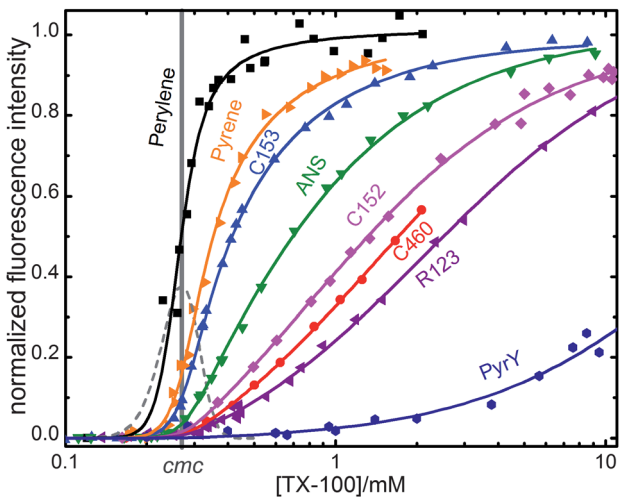

Fig. 6 Normalized fluorescence emission intensity of several dyes in aqueous solutions of TX100 as a function of surfactant concentration, $F_{norm} = (F - F_f)/(F_b - F_f)$. Continuous curves are results of a global fit of eqn (16) and (4)–(7) with fixed values of $cmc = 0.27$ mM and $r = 0.15$. The excitation and emission wavelengths and the ratios F_b/F_f are given in Table 1. Note the logarithmic concentration scale. This figure with a linear concentration scale is given in the ESI.† The dashed grey line is the relative second derivative of $[S_1]$ (eqn (2)) in arbitrary units with a transition width $\sigma = r \times cmc$.

Determination of the *cmc*

It is common practice to determine the *cmc* of a surfactant solution from the dye fluorescence with graphical methods.[10,24] Oversimplifying, it is in general assumed that the dye is sufficiently hydrophobic so that, once micelles are formed, all dye molecules are immediately incorporated into the micelles, with a negligible concentration of free dye in the aqueous phase. The *cmc* is then identified as the concentration at the onset of a change in absorbance or emission intensity in a titration series. Plots of the fluorescence intensity (or dye absorbance) at a given wavelength *versus* the logarithm of the concentration typically show an approximately linear region around their inflection point (see Fig. 6). The intersection of a straight line drawn through this region with the horizontal line defined by the points well below the *cmc* is then taken as the *cmc*. However, the selection of the points for the "linear" region is highly subjective, even in the case that the linear regression and the intersection are calculated analytically. The value of the *cmc* determined with

Table 1 Binding equilibrium constants K of dyes in aqueous solutions of TX100 and critical micelle concentration *cmc* of TX100 determined from fluorescence titrations of the dyes

Dye	K‡/10^3 M^{-1}	*cmc*[b]/mM	λ_{ex}, λ_{em}[c]/nm	F_b/F_f[d]	$[D]_0/M$	$\bar{i}_0$[f]
Perylene	$(10 \pm 2) \times 10^3$[a]	0.25	405, 444	8	—	—
Pyrene	$(2 \pm 1) \times 10^3$[a]	0.26	319, 383	5	2×10^{-7}	0.4
C153	970 ± 20[b]	0.290	380, 525	6	$<5 \times 10^{-8}$	<0.05
ANS	380 ± 20[b]	0.288	350, 420	125	2×10^{-6}	0.8
C152[g]	140 ± 15[b]	0.22	405, 510	4	$<5 \times 10^{-7}$	<0.07
C460[g]	82 ± 5[b]	0.25	380, 450	12	3×10^{-7}	0.03
R123[g]	60 ± 5[b]	0.24	488, 525	0.3	2×10^{-8}	0.001
PyrY[e]	4 ± 1[a]	—	515, 560	0.5	1×10^{-6}	0.004

[a] Estimated from the global fit shown in Fig. 6. [b] Determined from fits at several wavelengths of titrations of individual dyes as shown for ANS (Fig. 3) and C153 (Fig. 5) and in the ESI. [c] Excitation and emission wavelengths used in data of Fig. 6. [d] Ratio of the limiting fluorescence emission intensities F_b/F_f of free and bound dye at λ_{em}. [e] Determined from a concentration range extended up to [TX100] = 50 mM. [f] Initial mean occupation number $\bar{i}_0 = [D]_0 K$ (eqn (10)). [g] See figures in the ESI.

this graphical method from fluorescence intensity titrations dye was found to deviate systematically from those determined from direct properties, such as surface tension or conductivity of the surfactants.[10,59] Fig. 7(a) shows the same titration data as Fig. 6, but overlaid with linear regressions of the data in the approximately linear region of each of the curves. The straight lines and the intersections with the horizontal line (black dots) were determined analytically. The *cmc* values determined by this method depend strongly on the affinity of the dye to the micelles, with values between 0.2 mM (Perylene) and 0.4 mM (R123). In Fig. 7(b) we compare the dependence of the *cmc*-values determined with the two methods on the binding constants K of each of the dyes (note the logarithmic scale in K). Panel (b) shows a clear systematic trend both in the value and in the uncertainty of the *cmc* determined by the graphical method (black dots). In contrast, the *cmc*-values determined from fits with the proposed concentration model (blue triangles) show a much smaller dependence on the dye used, with a weighted mean value of 0.276 ± 0.008 mM, which coincides with the value from direct TX100 absorbance. The proposed concentration model takes into account the binding equilibrium of the dyes and yields consistent values for the *cmc* despite the huge difference in the values of the binding equilibrium constants.

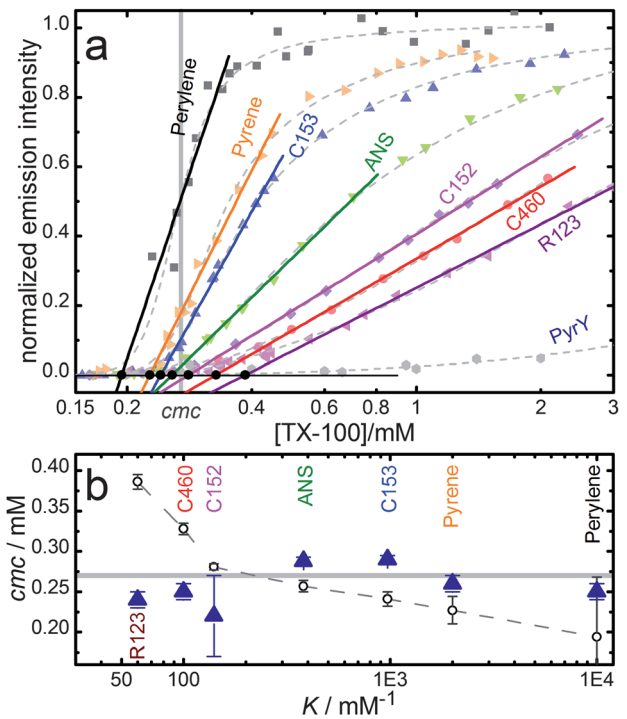

Fig. 7 Influence of the binding equilibrium on the determination of the *cmc* by different methods. (a) Filled symbols and grey dashed lines: same fluorescence intensities as in Fig. 6. Straight lines: linear regression of the approximately linear part of the fluorescence intensity. Black dots: intersections with the horizontal straight line taken by this graphical method as the *cmc*. (b) Dependence of the *cmc*-values estimated with the two methods on the binding constant K (Table 1). Blue triangles: fits of concentration model eqn (4)–(7) and (16) as in Fig. 6. Circles: graphical method based on the intersection of straight lines given in panel a. Grey horizontal line: *cmc* = 0.27 mM, estimated from the direct TX100 absorbance (Fig. 1 and 2).

It is important to recognize that the deviations between the true *cmc* and the values determined by the graphical method are intrinsic to the graphical method and not due to impurities or measurement uncertainties. The deviations cannot be easily corrected and it is also not obvious for a given surfactant which dye will yield the best *cmc* estimation. We therefore strongly discourage the use of such a graphical method. In order to obtain consistent and reproducible values of the *cmc* from moderately hydrophobic dyes we recommend therefore the use of an analytical model that takes into account the binding equilibrium of the dye, such as that of eqn (16) and (4)–(7). This analytical model avoids the subjectivity of the graphical methods and uses the full experimental dataset, including the values near the *cmc*. This fit procedure can be easily implemented for global fitting and automated analysis. An analytical model such as the one presented here makes it also possible to apply principal component analysis (PCA) and global analysis to the whole spectral dataset and to obtain the number of spectral components and their pure emission spectra.

Fluorescence correlation spectroscopy

In previous contributions we presented how to use FCS for the determination of dynamic rate constants of the dye-exchange

process with micelles.[8,17,18] Nevertheless, the high sensitivity of FCS to the size of the diffusing fluorescent particles makes it also very suitable for the estimation of the *cmc*, the size of the micelles, the formation of premicellar aggregates and other micellar properties.[12–15] In this contribution we focus on the analysis of the changes in the translational diffusion of the dyes R123 and C152 in TX100 solutions as measured by FCS.

Fig. 8 shows normalized FCS curves of R123 in aqueous solutions of TX100 with [TX100] = 0–18 mM. Up to the *cmc* the correlation curves overlap perfectly with that of the free dye. They show a diffusion term at about 250 μs, and a small triplet term around 3 μs with the expected irradiance-dependent amplitude.

Above the *cmc* the diffusion term shifts to higher correlation times (up to 1100 μs at [TX100] = 18 mM) without any further change in its shape. The additional irradiance-independent term below 10 μs reflects the fast flicker in the brightness of the dye during its dynamic exchange between water and the micelles, which depends on the dynamic rate constants of association and dissociation, k_+ and k_-, as given in eqn (11).[8,17,18]

Individual fits of the correlation curves of R123 (Fig. 8) and C152 (see ESI†) with the correlation function for one diffusing species, triplet and binding dynamics (eqn (21)) in the full time range are excellent and give the mean diffusion times shown for R123 in the inset of Fig. 8 (for C152 see the ESI†). The precision of the FCS data of R123 is much higher because this dye is much brighter and photostable than C152.

Below the *cmc* the measured diffusion times are identical to those of the free dyes. Above the *cmc* still only one species is observed, but with a mean diffusion time which increases with the surfactant concentration. As expected, even around the *cmc*, free dye and bound dye are not observed separately as two species because of their fast exchange between free and bound states during the time the dye needs to diffuse through the sample volume. The slow limit τ_R^0 of the relaxation time of this fast exchange can be estimated with eqn (24) from the binding constants of the dyes (see Table 1).[8] One obtains limits of $\tau_R^0 \approx$ 60 μs for R123 and $\tau_R^0 \approx$ 140 μs for C152, both faster than the diffusion times even of the pure dyes.

The individual mean diffusion times $\bar{\tau}_D$ can in turn be fitted with the fast exchange equilibrium model of eqn (23) with eqn (4)–(7) for the micelle concentration (see the inset of Fig. 8 and the ESI†). The fits are excellent (see parameters in Table 2). The same parameter values are obtained with global target fits of eqn (21), (23), and (4)–(7) directly to the full correlation curves.[36]

The binding constants *K* obtained from these fits of the FCS data with the fast exchange model are in very good agreement with those obtained before from the bulk fluorescence intensity titrations (Table 1). Despite the considerable extrapolation above the highest measured TX100 concentration a relatively precise value for the limiting diffusion time (τ_{Db}) of bound R123 is obtained. The *cmc* can be well recovered from the R123 data. The uncertainty in the C152 data is much higher, both due to its lower brightness and photostability and because of the low binding equilibrium constant. For the individual fit of the C152 data we therefore fixed the value of the *cmc* to that obtained directly from the TX100 absorbance.

Using the known diffusion coefficients of the free dyes as a reference, the diffusion times $\bar{\tau}_D$ can be converted to translational diffusion coefficients $\bar{D}$ (eqn (18)), which are independent of the detection volume (see Fig. 9). This conversion leads to non-constant uncertainties in $\bar{D}$, which are therefore used as weights in the fits.

The translational diffusion coefficient of free C152 is slightly higher than that of free R123, as expected from the smaller size of C152. Up to the *cmc* the diffusion coefficients of both dyes are

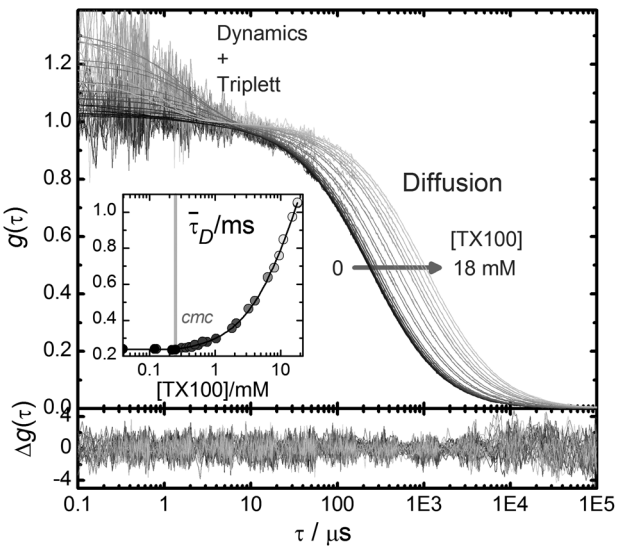

Fig. 8 Normalized fluorescence correlation curves (FCS) of R123 in TX100 solutions with [TX100] = 0–18 mM. Noisy curves are the experimental data. Thin smooth curves are fits of eqn (21) with the mean diffusion times $\bar{\tau}_D$ which are shown as circles in the inset. The continuous line in the inset is the fit of eqn (23) to the values of $\bar{\tau}_D$ obtained from the individual fits. The fit parameters are given in Table 2 and in the text.

Table 2 Results of fits of the FCS titrations from Fig. 8 and 9 for R123, C152 and Chol-Bp[c]

	R123	C152	Chol-Bp
$K/10^3$ M^{-1}	56 ± 2	143 ± 14	—
λ_{ex}/nm	488	405	488
cmc/mM	0.25 ± 0.02	(0.27)	—
τ_{Df}[a]/ms	0.237 ± 0.002	0.242 ± 0.005	—
τ_{Db}[a]/ms	1.97 ± 0.08	2.2 ± 0.5	1.85 ± 0.10
D_f[b]/10^{-10} m^2 s^{-1}	4.58 ± 0.01	5.1 ± 0.1	—
D_b[b]/10^{-10} m^2 s^{-1}	0.55 ± 0.02	0.55 ± 0.02	0.56 ± 0.02
R_{hf}/Å	5.2	4.7	—
R_{hb}/Å	44	44	43

[a] From global fits of eqn (21) and (23) to the full titration data. [b] From global fits of eqn (23) to the *D* values in Fig. 9 with common but free D_b. [c] All fits with a fixed value of $r = 0.15$. Values of *r* between 0.1 and 0.2 had no influence on the results indicated in this Table. The measured diffusion times τ_{Df} of free R123 and C152 are similar despite the smaller size of the latter because of the slightly bigger focus size at the excitation wavelength of 405 nm used for C152 as compared to the size at 488 nm used to excite R123. The translational diffusion coefficients and hydrodynamic radii are absolute values, independent of the focus size.

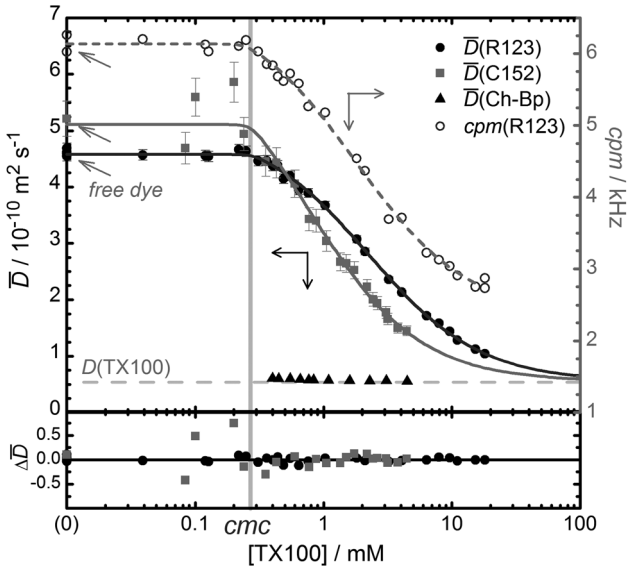

Fig. 9 Upper panel, left scale: mean translational diffusion constants D of the dyes R123 (black circles), C152 (grey squares) and Bdp-Chol (black triangles) in aqueous TX100 solutions, determined from the FCS data shown in Fig. 8 and ESI.† Smooth lines represent the global fit of eqn (22) to the R123 and C152 data with the parameters given in Table 2. The open circles are the fluorescence intensity of R123 (counts per second per molecule, *cpm*, right scale) and the fit of eqn (16) (dashed line). Lower panel: residuals of the global fit to D. The fit parameters are given in Table 2 and in the text.

constant and equal to those of the free dyes. Above the *cmc* the mean diffusion coefficients decrease due to the increasing fraction of the time a dye is bound to the slower diffusing micelle. At high TX100 concentration both curves tend to the same limiting diffusion coefficient, that of the TX100 micelle. This value of $D_b = (0.55 \pm 0.02)\ 10^{-10}$ m^2 s^{-1} obtained in a global fit of both dyes coincides excellently with the reported value of $D_b = 0.54\ 10^{-10}$ m^2 s^{-1} obtained from Dynamic Light Scattering.[60]

We also measured under the same conditions FCS curves of a highly hydrophobic cholesterol labelled with the dye Bodipy (Bdp-Chol) at different TX100 concentrations (black triangles in Fig. 9). In pure water, not even nanomolar FCS concentrations of Bdp-Chol could be dissolved. In the presence of TX100 at concentrations below the *cmc* big and polydisperse aggregates were observed. However, immediately above the *cmc* stable solutions were obtained with a single diffusion term at $\bar{\tau}_D$ = 1.9 ms, which did not increase further at higher TX100 concentrations, indicating that all Bdp-Chol was incorporated into micelles. The corresponding translational diffusion coefficient (see Table 2) coincides well with the one determined from the fits to R123 and C152 and with the mentioned published value. The incorporation of the dyes R123, C152 and Chol-Bp into the micelles does not have a significant influence on the diffusion coefficient or hydrodynamic radius of the TX100 micelles, as opposed to observations with other guests.[12]

It should also be noted that the diffusion coefficients measured around the *cmc* can be satisfactorily explained by the proposed concentration model. At least with these two dyes of low hydrophobicity we do not observe dye-surfactant aggregates, premicellar aggregates or nucleation of micelles. However, until now, we did not obtain FCS data around the *cmc* from more hydrophobic dyes that may induce these effects more effectively.

The fluorescence intensity observed in the FCS titrations for R123 at different TX100 concentrations is also represented in Fig. 9 (open circles). From the total registered intensity and the mean number of R123 molecules present in the sample volume (typically 4–10 molecules) the fluorescence intensity detected from each dye molecule is calculated (fluorescence counts per second per molecule, *cpm*). This intensity is the single molecule equivalent to the bulk fluorescence intensity of R123 represented in Fig. 6 and can be fitted with the same eqn (16) and (4)–(7), giving the same value of $K = (57 \pm 2) \times 10^3$ M^{-1}.

Experimental section

Materials

Dyes used: Perylene (Fluka 77341, CAS 198-55-0, Mw = 252.32); Pyrene (Aldrich 42642-3 (99%), CAS 129-00-0, Mw = 202.26); C153 (Coumarin 153, Aldrich 546186, CAS 53518-18-6, Mw = 309.29); ANS (2-anilinonaphthalene-6-sulfonic acid, Molecular Probes A-50, CAS 20096-53-1, Mw = 299.34); C152 (Coumarin 152, Aldrich 363324 (98%), CAS 53518-14-2, Mw = 257.22); C460 (Coumarin 460, 7-diethylamino-4-methylcoumarin (99%), Aldrich D87759, CAS 91-44-1, Mw = 231.3); R123 (Rhodamine123, Sigma R8004, CAS 62669-70-9, 380.83); PyrY (pyroninY, Aldrich 213519 (53%), CAS 92-32-0, 302.81); Bdp-Chol (TopFluor (Bodipy) cholesterol, 23-(dipyrromethemeboron difluoride)-24-norcholesterol, Avanti 810255P, CAS 878557-19-8, Mw 576.61). All dyes were used without further purification. The surfactant TX100 (Triton X-100, Fluka 93426, CAS 9002-93-1, Mw = 646.85) was checked for potential fluorescence impurities and was used without further purification. Solutions were prepared using Milli-Q water. Dyes with very low solubility in pure water (Perylene, Pyrene and Bdp-Chol) were dissolved directly in aqueous TX100 solutions. In the case of perylene these solutions had to be filtered in order to avoid dye precipitation during the titrations.

For each dye a different TX100 stock solution was prepared, with an uncertainty of about 1% in the absolute TX100 concentration. This uncertainty propagates to all derived values, and defines the accuracy of the *cmc* and K values. This uncertainty is, however, not included in the errors given throughout the text, which indicates only the precision of the nonlinear fits.

Absorbance and fluorescence measurements

Absorbance spectra were recorded using quartz cells with an absorption path length of 10.0 mm in a Varian-Cary 300 spectrometer. The baseline was recorded with water in both sample and reference cells. Steady-state fluorescence measurements were performed with an Edinburgh-Instruments F900 spectrofluorimeter, equipped with a xenon lamp of 450 W as the excitation source. All experiments were carried out at 25 ± 1 °C.

FCS measurements

The FCS setup was described before.[18,61] A drop of each sample was deposited on a borosilicate coverslip (Menzel Gläser, NO. 1 DE) or in a well of a glass bottom microplate (Whatman Ltd.). The samples were excited through a microscope objective (Olympus, UPLSAPO 60xW/1.20, water immersion) by laser light at 405 nm or 489 nm. The fluorescence was collected by the same objective and passed through a pinhole (Thorlabs, $\varnothing = 100$ μm, US) and filtered by band-pass filters (Semrock, Brightline HC 525/45, US or AHF Analysentechnik, HQ550/100M, Germany) The output signals of avalanche photodiodes (MPD50CTC APD, $\varnothing = 50$ μm, MPD, Italy) were processed and stored by TCSPC-modules (SPC 132, Becker & Hickl GmbH, Berlin, Germany).

Typically 10 million photons were collected for each correlation curve. All measurements were performed at stabilized temperature, 25.0 ± 0.5 °C. The excitation power was typically $P = 120$ μW, the mean irradiance $I_0/2 = 9$ kW cm^{-2}.[55]

The detection volumes were calibrated at 489 nm with Rhodamine 123 and at 405 nm with C152: w_{xy} (405 nm) = 0.70 μm and w_{xy} (488 nm) = 0.66 μm@488 nm. The diffusion coefficient D (R123, 25 °C) = (4.6 ± 0.4) × 10^{-10} m^2 s^{-1} was estimated from PFG-NMR[62] and dual-focus FCS[63] data.[64] The diffusion coefficient D (C152, 25 °C) = (5.2 ± 0.6) × 10^{-10} m^2 s^{-1} has been taken from Bordello *et al.*[18] The diffusion coefficients are given for 25 °C.

The detection volumes were selected large enough in order to ensure at least a 50-fold temporal separation between the diffusional terms and the fast terms of the binding dynamics and the triplet state blinking. Power series were performed both for the free dye and at the highest surfactant concentration in order to determine the photobleaching limits.[18]

Conclusions

We present for the first time a practical quantitative model for the surfactant concentration dependence of the fluorescence intensity and the translational diffusion coefficients of dyes in micellar solutions. The model yields excellent fits of the experimental data, especially also around and below the *cmc*. We show how this model can be used for the precise determination of the binding equilibrium constants of dyes of very different hydrophobicity.

We strongly advise not to use subjective graphical methods for the determination of the *cmc* of surfactant solutions. We demonstrate that the intersection of two straight lines in plots of the fluorescence emission intensity of a dye *versus* the surfactant concentration depends strongly on the affinity of the dye to the micelles and, of course, on the chosen interval and the quality of the data. The same applies to other properties, such as the diffusion coefficient or absorbance.

Data analysis based on a concentration model such as that presented in this contribution can lead to objective and consistent values of the *cmc* which are much less dependent on the technique or on subjective decisions. Furthermore, this type of analysis is easily implemented in commercial fitting software and can be used for global and automated analysis, also in high throughput applications. It is not limited to fluorescence intensity and diffusion coefficients, but can also be applied to ratiometric data and to other properties which depend directly on the concentration of monomeric and micellised surfactants.

Acknowledgements

J.B., S.F., and L.P. thank the Ministerio de Ciencia e Innovación, the Xunta de Galicia, and the Gil Dávila Foundation for their research scholarships. M.N. and W.A. thank the Ministerio de Ciencia e Innovación and the Xunta de Galicia for their financial support (CTQ2010-21369, INCITE09262304PR, IN845B-2010/094, INCITE09E2R209064ES, CN2013/314).

Notes and references

1 T. F. Tadros, *Applied surfactants: principles and applications*, Wiley-VCH Verlag GmbH & Co. KGaA, Weinheim, 2005.
2 M. J. Rosen and J. T. Kunjappu, *Surfactants and interfacial phenomena*, John Wiley & Sons, Inc., New Jersey, 2012.
3 A. M. Seddon, P. Curnow and P. J. Booth, *Biochim. Biophys. Acta, Biomembr.*, 2004, **1666**, 105–117.
4 E. Blanco, C. W. Kessinger, B. D. Sumer and J. Gao, *Exp. Biol. Med.*, 2009, **234**, 123–131.
5 P. Stano, *Syst. Biol. Synth. Biol.*, 2010, **4**, 149–156.
6 C. S. Dunaway, S. D. Christian and J. F. Scamehorn, in *Solubilization in Surfactant Aggregates, Surfactant Science Series*, ed. S. D. Christian and J. F. Scamehorn, Marcel Dekker, New York, 1995, vol. 55, pp. 3–31.
7 R. Zana, in *Dynamics of Surfactant Self-Assemblies: Micelles, Microemulsions, Vesicles, and Lyotropic Phases*, ed. R. Zana, Taylor & Francis/CRC Press, Boca Raton, 2005.
8 M. Novo, S. Felekyan, C. A. M. Seidel and W. Al-Soufi, *J. Phys. Chem. B*, 2007, **111**, 3614–3624.
9 K. P. Ananthapadmanabhan, E. D. Goddard, N. J. Turro and P. L. Kuo, *Langmuir*, 1985, **1**, 352–355.
10 A. Patist, in *Handbook of Applied Surface and Colloid Chemistry*, ed. K. Holmberg, John Wiley & Sons, New York, 2001, p. 239.
11 Y. Nakahara, T. Kida, Y. Nakatsuji and M. Akashi, *Langmuir*, 2005, **21**, 6688–6695.
12 M. A. Hink, A. Van Hoek and A. J. W. G. Visser, *Langmuir*, 1999, **15**, 992–997.
13 H. Zettl, Y. Portnoy, M. Gottlieb and G. Krausch, *J. Phys. Chem. B*, 2005, **109**, 13397–13401.
14 L. Yu, M. Tan, B. Ho, J. L. Ding and T. Wohland, *Anal. Chim. Acta*, 2006, **556**, 216–225.
15 F. Luschtinetz and C. Dosche, *J. Colloid Interface Sci.*, 2009, **338**, 312–315.
16 A. Techen, C. Hille, C. Dosche and M. U. Kumke, *J. Colloid Interface Sci.*, 2012, **377**, 251–261.
17 W. Al-Soufi, B. Reija, S. Felekyan, C. A. Seidel and M. Novo, *ChemPhysChem*, 2008, **9**, 1819–1827.
18 J. Bordello, M. Novo and W. Al-Soufi, *J. Colloid Interface Sci.*, 2010, **345**, 369–376.
19 M. Deumié and M. El Baraka, *J. Photochem. Photobiol., A*, 1993, **74**, 255–266.

20 P. Pal, H. Zeng, G. Durocher, D. Girard, R. Giasson, L. Blanchard, L. Gaboury and L. Villeneuve, *J. Photochem. Photobiol., A*, 1996, **98**, 65–72.
21 J. C. Micheau, G. V. Zakharova and A. K. Chibisov, *Phys. Chem. Chem. Phys.*, 2004, **6**, 2420–2425.
22 R. Barnadas-Rodríguez and J. Estelrich, *J. Phys. Chem. B*, 2009, **113**, 1972–1982.
23 S. Freire, J. Bordello, D. Granadero, W. Al Soufi and M. Novo, *Photochem. Photobiol. Sci.*, 2010, **9**, 687–696.
24 P. Mukerjee and K. J. Mysels, *Critical Micelle Concentrations of Aqueous Surfactant Systems*, NIST National Institute of Standards and Technology, Washington D.C., USA, 1971.
25 W. Al-Soufi, L. Piñeiro and M. Novo, *J. Colloid Interface Sci.*, 2012, **370**, 102–110.
26 S. H. Brooks, A. Berthod, B. A. Kirsch and J. G. Dorsey, *Anal. Chim. Acta*, 1988, **209**, 111–121.
27 G. B. Behera, B. K. Mishra, P. K. Behera and M. Panda, *Adv. Colloid Interface Sci.*, 1999, **82**, 1–42.
28 J. Phillips, *Trans. Faraday Soc.*, 1955, **51**, 561–569.
29 I. García-Mateos, M. Mercedes Velázquez and L. J. Rodríguez, *Langmuir*, 1990, **6**, 1078–1083.
30 S. Morisada and H. Shinto, *J. Phys. Chem. B*, 2010, **114**, 6337–6343.
31 R. Hadgiivanova and H. Diamant, *J. Phys. Chem. B*, 2007, **111**, 8854–8859.
32 K. Kalyanasundaram, *Photochemistry in Microheterogeneous Systems*, Academic Press, New York, 1987.
33 J. K. Thomas, *Chem. Rev.*, 1980, **80**, 283–299.
34 J. Widengren and R. Rigler, *Cell. Mol. Biol.*, 1998, **44**, 857–879.
35 R. Rigler and E. S. Elson, *Fluorescence correlation spectroscopy: theory and applications*, Springer Verlag, Berlin, 2001.
36 W. Al-Soufi, B. Reija, M. Novo, S. Felekyan, R. Kühnemuth and C. A. M. Seidel, *J. Am. Chem. Soc.*, 2005, **127**, 8775–8784.
37 K. Kalyanasundaram and J. Thomas, in *Micellization, Solubilization, and Microemulsions*, ed. K. L. Mittal, Springer, US, 1977, pp. 569–588.
38 F. G. Sánchez and C. C. Ruiz, *J. Lumin.*, 1993, **55**, 321–325.
39 H. Om, G. A. Baker, K. Behera, V. Kumar, K. K. Verma and S. Pandey, *ChemPhysChem*, 2010, **11**, 2510–2513.
40 U. Anand, C. Jash and S. Mukherjee, *J. Colloid Interface Sci.*, 2011, **364**, 400–406.
41 W. Al-Soufi, M. Novo, M. Mosquera and F. Rodríguez-Prieto, *Rev. Fluoresc.*, 2011, **2009**, 23–45.
42 W. Al-Soufi, M. Novo and M. Mosquera, *Appl. Spectrosc.*, 2001, **55**, 630–636.
43 J. R. Lakowicz, *Principles of Fluorescence Spectroscopy*, Springer, USA, 2006.
44 H. C. Chiang and A. Lukton, *J. Phys. Chem.*, 1975, **79**, 1935–1939.
45 K. Birdi, H. Singh and S. Dalsager, *J. Phys. Chem.*, 1979, **83**, 2733–2737.
46 E. De Vendittis, G. Palumbo, G. Parlato and V. Bocchini, *Anal. Biochem.*, 1981, **115**, 278–286.
47 E. Abuin, *J. Colloid Interface Sci.*, 1997, **186**, 332–338.
48 P. Griffiths, J. Roe, B. Bales, A. Pitt and A. Howe, *Langmuir*, 2000, **16**, 8248–8254.
49 N. Memon, A. Balouch and W. L. Hinze, in *Encyclopedia of Analytical Chemistry*, ed. R. A. Meyers, John Wiley & Sons, Ltd, US, 2006.
50 S. A. Moore, A. A. Harris and R. M. Palepu, *Fluid Phase Equilib.*, 2007, **251**, 110–113.
51 A. Accardo, D. Tesauro, L. Del Pozzo, G. Mangiapia, L. Paduano and G. Morelli, *J. Pept. Sci.*, 2008, **14**, 903–910.
52 P. Castellazzi, G. Mercier and J. Blais, *Water, Air, Soil Pollut.*, 2012, **223**, 337–349.
53 B. D. Wagner, *Molecules*, 2009, **14**, 210–237.
54 B. Valeur, *Molecular Fluorescence: Principles and Applications*, Wiley-VCH, Germany, 2002.
55 C. Eggeling, J. Widengren, R. Rigler and C. A. M. Seidel, *Anal. Chem.*, 1998, **70**, 2651–2659.
56 S. J. Yunes, N. D. Gillitt and C. A. Bunton, *J. Colloid Interface Sci.*, 2005, **281**, 482–487.
57 M. Sowmiya, A. Tiwari and S. Saha, *J. Colloid Interface Sci.*, 2010, **344**, 97.
58 D. LeBard, B. Levine, R. DeVane, W. Shinoda and M. Klein, *Chem. Phys. Lett.*, 2012, **522**, 38–42.
59 A. Patist, S. S. Bhagwat, K. W. Penfield, P. Aikens and D. O. Shah, *J. Surfactants Deterg.*, 2000, **3**, 53–58.
60 G. D. J. Phillies, J. Stott and S. Z. Ren, *J. Phys. Chem.*, 1993, **97**, 11563–11568.
61 D. Granadero, J. Bordello, M. J. Pérez-Alvite, M. Novo and W. Al-Soufi, *Int. J. Mol. Sci.*, 2010, **11**, 173–188.
62 P. O. Gendron, F. Avaltroni and K. J. Wilkinson, *J. Fluoresc.*, 2008, **18**, 1093–1101.
63 C. Muller, A. Loman, V. Pacheco, F. Koberling, D. Willbold and W. Richtering, *Europhys. Lett.*, 2008, 83.
64 P. Kapusta, *Absolute Diffusion Coefficients: Compilation of Reference Data for FCS Calibration*, Picoquant Application Note, 2010.

